The Effect of Confined Space on the Growth of Naphthalenic Species in a Chabazite-Type Catalyst: A Molecular Modeling Study

6 AUTHORS, INCLUDING:

Karen Hemelsoet
Ghent University
56 PUBLICATIONS **874** CITATIONS

SEE PROFILE

Matthias Vandichel
Ghent University
36 PUBLICATIONS **658** CITATIONS

SEE PROFILE

Michel Waroquier
Ghent University
417 PUBLICATIONS **8,266** CITATIONS

SEE PROFILE

The Effect of Confined Space on the Growth of Naphthalenic Species in a Chabazite-Type Catalyst: A Molecular Modeling Study

Karen Hemelsoet,* Arno Nollet, Matthias Vandichel, David Lesthaeghe, Veronique Van Speybroeck,* and Michel Waroquier[a]

Methylation reactions of naphthalenic species over the acidic microporous zeolite with chabazite topology have been investigated by means of two-layered ab initio computations. Large cluster results combined with van der Waals contributions provide thermodynamic and kinetic results of successive methylation steps. The growth of fused bicyclic species is important as these can act as hydrocarbon pool species within the methanol-to-olefin (MTO) process, but ultimately leads to the deactivation of the catalyst. The influence of the confined space of the zeolite pore on the resulting transition state or product shape selectivity is investigated in detail.

Introduction

The increasing demand for light olefins in the petrochemical industry, combined with the limited reserves of crude oil have raised interest in the methanol-to-olefin (MTO) process.[1,2] This process is the transformation of methanol (often made from natural gas or coal through synthesis gas) into light olefins (i.e., ethene and propene) over microporous solid acids, such as zeolites and zeotype materials. Silicoaluminophosphate with a CHA topology (H-SAPO-34) and H-ZSM-5 are the most applied and studied catalysts for the MTO process. The architectural characteristics of the CHA topology are optimal for commercialization as the 8-ring narrow windows provide selectivity towards small molecules such as ethene and propene.[3] Recently, other promising catalysts were tested, such as ZSM-22.[4,5] Particular shape selectivity of this catalyst results in a unique product spectrum, that is, branched C_{5+} species are mainly formed. In the last decades, the complex reaction mechanism of the MTO process has been intensely debated,[6–8] but experimental and computational findings have finally confirmed the hydrocarbon pool (HP) mechanism. In this hypothesis, organic reaction centers act as cocatalysts inside the zeolite pores.[9–11] The actual active catalyst is thus the combined organic–inorganic supramolecular complex of the HP and zeolite framework. The MTO conversion results from the repeated methylation of the organic compounds and cations derived thereof, followed by olefin elimination, which forms a full catalytic cycle.

Aromatics, typically polymethylbenzenes, and alkenes,[12–14] were so far found to be crucial HP species, differentiating between the aromatic and alkene routes, respectively. It can not be ruled out, however, that other HP species are also active. The aromatic route comprises the paring and sidechain mechanisms. The latter mechanism involves the deprotonation of an alkyl group on an alkylbenzenium species and the formation of an exocyclic double bond. This double bond is further methylated, which reforms a benzenium ion with a higher alkyl chain. The higher alkyl chains are subsequently eliminated as alkenes. The paring mechanism involves ring contractions or expansions to extend an alkyl group on the cationic species. It is currently understood that ethene is predominantly formed from the lower methylbenzenes, whereas propene formation is favored by methylbenzenes with four to six methyl groups. Modeling results combined with experimental findings recently led to the first example of a complete cycle in H-ZSM-5.[15] The alkene-based cycle was also studied in this catalyst, which indicated that this route contributes insignificantly to ethene, but is a highly relevant mode of propene formation.[12–14] The role of branched organics as the active species is also under investigation. The high selectivity to triptane in another methanol conversion process, catalyzed by ZnI_2 and InI_3, was recently reported.[16] All recent studies have enforced our vision that the MTO conversion is a very complex process during which various routes occur simultaneously.

To obtain additional insight, it is important to isolate one particular parameter at a time. Theoretical calculations are ideally suited to achieve this goal.[17] In this contribution, we investigate the effects of confined spaces on the growth of the naphthalenic species. Their role during the MTO process is not straightforward. They might be important in active routes towards formation of olefins but also in passive routes, which

[a] Dr. K. Hemelsoet, A. Nollet,+ M. Vandichel, Dr. D. Lesthaeghe,
Prof. Dr. V. Van Speybroeck, Prof. Dr. M. Waroquier
Center for Molecular Modeling, QCMM Alliance Ghent-Brussels
Ghent University, Technologiepark 903, 9052 Zwijnaarde (Belgium)
Fax: (+32) 9-264-66-97
E-mail: karen.hemelsoet@ugent.be
        veronique.vanspeybroeck@ugent.be

[+] Present address:
Shell/NAM, Schepersmaat 2, Postbus 28000
9400 HH Assen (The Netherlands)

lead to the deactivation of the catalyst. We focus on a high-silicon chabazite catalyst for which we have developed a well-established procedure to calculate the kinetics from first principles.[18] We also found that methylations of benzene-like species could be dramatically sped up in the chabazite topology.[18] Important geometrical characteristics of this CHA catalyst are illustrated in Figure 1. The methylated species are quite
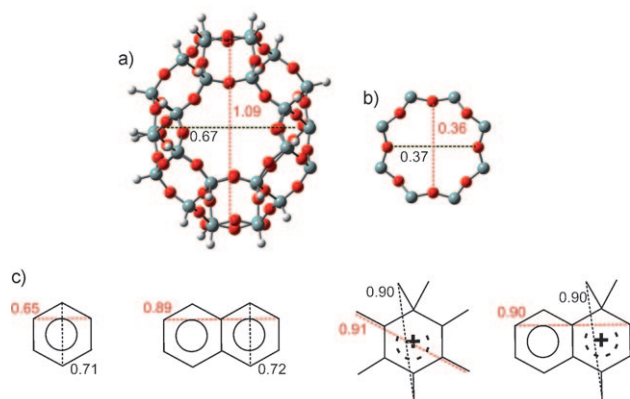

Figure 1. Geometrical characteristics of a) the CHA zeolite pore, b) 8-membered ring window, and c) some illustrative HP species. Free diameters (taking into account van der Waals radii, that is, 0.11 nm for H, 0.17 nm for C and 0.15 nm for O) are indicated in nm.

bulky compared to the free pore diameters and thus the stabilizing and steric effects of the zeolite topology are essential. Interestingly, the naphthalenic species investigated here are of the same size as the traditional benzenic HP species, such as the heptamethylbenzenium ion. The confinement effects of the zeolite pore might nevertheless be different, especially in the case of voluminous transition state structures.

A previous theoretical study by our group elucidated the influence of zeolite topology, which compared the MFI, CHA, and BEA frameworks for the crucial *ipso*-methylation reaction of hexamethylbenzene.[18] The following order of reactivity according to topology was found: CHA ≫ MFI > BEA. Park and Seo compared the performance of CHA, LTA, MFI, BEA, MOR, and FAU topologies by using in situ IR spectroscopy.[19] The number of strong acidic sites within the zeolite and the topology were found to be determining factors for the deactivation. Seo and co-workers investigated the effects of shape and size of the cage on the deactivation during the MTO process, comparing four eight-membered ring molecular sieves with an Si/Al molar ratio of 5–6:1[20] Although the initial activity and selectivity of the catalysts were very similar, the deactivation behavior differed to a large extent and the following order was found: CHA ≪ LTA < ERI < UFI. UV/Vis spectra indicated that the formation of large polycyclic aromatics in the CHA cages for a short time was not detectable.[20] Bleken et al. recently addressed the influence of acid strength, comparing H-SAPO-34 with the more acidic H-SSZ-13 variant at similar conditions.[21] Both catalysts were found to act similarly, however, a lower optimal operation temperature and increased ethene/propene ratio were found for H-SSZ-13.

The role of naphthalenic species during the MTO process was experimentally investigated by Haw and co-workers. Using the cryogenic grinding method,[22] it was found that in SAPO-34, methylnaphthalenes become significantly present after the addition of 1 or 2 mL of methanol for 0.3 g of catalyst. A careful comparison showed the naphthalenic species to be approximately one third as active as their benzenic counterparts. However, a higher ethene selectivity was obtained,[23] which could be related to the observation that methylnaphthalenes in H-SAPO-34 never contain more than four methyl groups.[24] Methylphenanthrenes are restricted to two groups, whereas their catalytic activity is almost non-existent. They are still able to age to pyrene with no methyl groups, which is seen as the final state of the degenerated catalyst cage.[24] Bjørgen and co-workers investigated the formation of coke precursors from hexamethylbenzene reacting over H-beta at 325 °C. They found that the large hexamethylnaphthalene compounds could easily be formed from dihydrotrimethylnaphthalene by methylations and hydrogen transfers.[25] In general, the deactivation was fast. The latter observations relate to the deactivation of the catalyst by coking, which naturally influences both activity and selectivity. Many uncertainties regarding this deactivation process remain, partially due to the generally poor characterization of coke. Bordiga et al. applied ex situ spectroscopic techniques (i.e., DR-UV/Vis and IR) to study the nature of the carbonaceous species formed in H-ZSM-5.[26] They found that methylated aromatic carbocationic species slowly evolve into precursors of graphitic coke. Weckhuysen et al. recently focused on the differences between the coking behavior in H-ZSM-5 and H-SAPO-34, by using in situ UV/Vis spectroscopy combined with confocal fluorescence microspectroscopy.[27] Graphitic coke on H-ZSM-5 crystals is initially formed at the edges of the crystal, whereas in H-SAPO-34 aromatic coke compounds are mainly formed inside the crystals. A recent study on the deactivation of H-SAPO-34 by Olsbye and co-workers, using isotopic switch experiments, revealed that an increased ethene/propene ratio results from product shape selectivity rather than transition-state shape selectivity as the diffusion of small molecules are hindered through the presence of bulky species inside the zeolite pores.[28]

Results and Discussion

Methylation scheme

To study the potential activity of the naphthalenic species during an active MTO cycle, we concentrated on the methylation reactions of the aromatic unit. This step was previously shown to be one of the slowest of the overall reaction cycle;[15] moreover, it is the crucial step before any olefin producing cycle (sidechain or paring) can be initiated. The influence of acidity, through comparison of the protonated aluminosilicate CHA and H-SAPO-34 catalysts, is the focus of another study. The overall studied reaction scheme consists of several types of methylations (Scheme 1). Firstly, a distinction is made between α and β sites (Scheme 1 and Scheme 2), defined by the position of the carbon atom undergoing electrophilic attack.
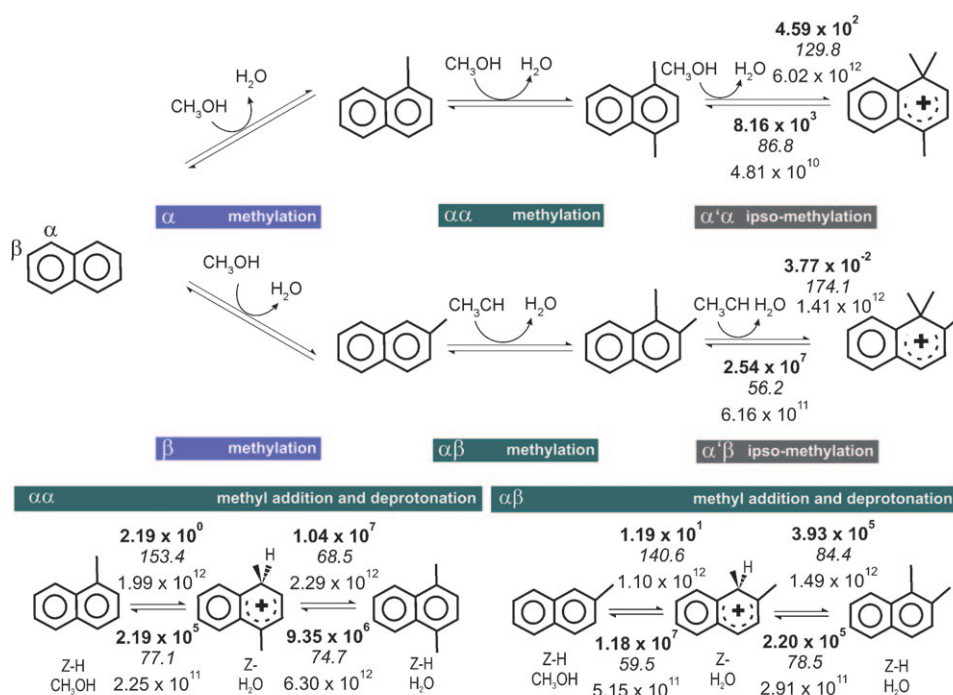
Scheme 1. Methylations and *ipso*-methylations of naphthalenic compounds; rate constants k at 670 K (bold) are given in s^{-1}, activation barriers E_a (italics) in $kJ\,mol^{-1}$, and pre-exponential factors A in s^{-1}.

Secondly, *ipso*-methylations are considered since the created *gem*-methylated species lead to the onset of the olefin-producing routes.[18] The growth of HP species within the confined space of a zeolite cage is represented by two routes resulting in the formation of a trimethylnaphthalenium ion (Scheme 1). The first route consists of three successive α-methylations. The first step is a normal α-methylation of naphthalene (α), followed by a second normal methylation step (αα), and thirdly an *ipso*-methylation (α′α). The second route consists of a normal β-methylation of naphthalene followed by a second

normal methylation step (αβ) and an *ipso*-methylation (α′β). Unlike many other theoretical studies, all of our conclusions are based on rate constants at the actual temperature of operation.

These values and the kinetic parameters derived in the 620 to 770 K temperature interval are given in Scheme 1 and Scheme 2. A new code developed in our group was used to efficiently perform the kinetic analysis.[29–31] Reaction barriers and reaction energies for all reaction steps are given in Table 1.

As shown previously for the MFI topology,[15] the stabilizing effect of the zeolite framework on carbenium ions leads to a stepwise methylation behavior as opposed to the concerted gas-phase results. A relatively slow methylation step is followed by a much faster deprotonation, which leads to a neutral aromatic and regeneration of an acidic site in the zeolite framework. The energy barriers at 0 K immediately reveal that there is a non-negligible effect of the confined space; the obtained values are relatively high.

The first methyl addition is more difficult compared to a second addition of a methyl group. At 670 K, $k_{\alpha\alpha}/k_\alpha$ equals 77 and $k_{\alpha\beta}/k_\beta$ equals 3. The α versus β results indicate that the position of the electrophilic attack is important ($k_\beta/k_\alpha = 122$, at 670 K), although not determining. The methylation at the β position is more hindered by the confinement of the pore, as the large organic compounds are pushed out of the chabazite cage. Moreover, this methylation results in a charged product
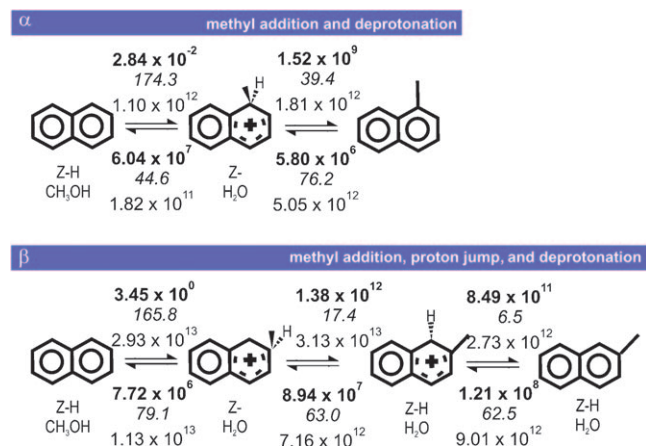
Scheme 2. First methylation (α and β) of naphthalene; rate constants k at 670 K (bold) are given in s^{-1}, activation barriers E_a (italics) in $kJ\,mol^{-1}$, and pre-exponential factors A in s^{-1}.

Table 1. Energy barriers $\Delta E^{\pm}$ and reaction energies ΔE_r (based on electronic energies at the ONIOM(b3lyp/dgtzvp:hf/dgtzvp) level) and corresponding van der Waals corrections. All values in $kJ\,mol^{-1}$.

	$\Delta E^{\pm}$	ΔE_r	vdW ($\Delta E^{\pm}$)	vdW (ΔE_r)
α methyl addition	171.7	126.3	−23.4	−15.9
β methyl addition	165.3	85.6	−18.3	−2.0
αα methyl addition	150.6	73.6	−18.3	−6.6
αβ methyl addition	138.3	78.9	−23.0	−8.1
β proton jump	23.3	−43.3	2.0	0.7
α deprotonation	49.6	−39.2	−2.9	2.9
β deprotonation	14.3	−57.7	1.1	−3.2
αα deprotonation	78.8	−8.5	−3.5	0.4
αβ deprotonation	93.9	1.8	−19.2	0.3
α′α *ipso* addition	127.5	40.6	−15.7	−3.4
α′β *ipso* addition	170.2	113.4	−30.2	−18.2
exocyclic deprotonation	96.2	48.3	−8.1	6.8
exocyclic methylation	197.9	162.7	−28.0	−35.6

species which can not directly be deprotonated due to an unfavorable position of the proton towards an oxygen atom near the aluminum (Scheme 2). A proton jump to a neighboring ring carbon atom is thus needed, which can then be followed by a deprotonation step. The calculated energetics and rate constants indicate that the barriers for this proton shift are very low (i.e., 23.3 kJ mol^{-1}), with a corresponding rate coefficient of 1.38×10^{12} s^{-1} at 670 K. Overall, the methyl additions exhibit high barriers and are highly endothermic leading to slow

reactions.

The α and $\alpha\alpha$ deprotonation reactions are found to be exothermic and the barriers are much lower. Comparison with previous work indicates that the average barrier for deprotonation of the bicyclic compounds is much higher compared to that of the benzenic species within an H-ZSM-5 zeolite.[15] The catalyst acidity (CHA > MFI[32]), proton affinity of the aromatic molecule,[33,34] and topology are responsible for these differences. The chabazite stabilizes the carbenium ions to a large extent[18] and thus deprotonation is less favorable compared to the MFI structure. β deprotonation has a very low barrier and occurs very fast. On the contrary, the $\alpha\beta$ deprotonation exhibits a higher barrier at 0 K since the methyl group at the β position prohibits the transition state structure to take on the optimal geometry. However, conduits, such as water and methanol, which are present inside the zeolite pores, assist the deprotonation. These reactions represent the fastest reaction type studied in this contribution.

For the *ipso*-methylation reactions, the influence of the zeolite confinement is also found to be important. The $\alpha'\alpha$ *ipso* reaction shows an energetically favorable transition-state geometry, whereas the transition state of $\alpha'\beta$ *ipso* reaction differs from the optimal geometry and the barrier increases (127.5 versus 170.2 kJ mol^{-1}). The $\alpha'\beta$-resulting cationic product species is less stabilized by the zeolite framework. The resulting effect on the rate coefficients is very large (difference of approximately four orders of magnitude at 670 K). In Figure 2, the optimized transition state structure of the $\alpha'\beta$ reaction is depicted.

Overall, the methyl addition reactions are found to be the rate-limiting step, which is in accordance with previous reports for the reactions of benzenic species in H-ZSM-5.[15]

Onset of the sidechain route

We previously detected the increased activity of the *ortho*-methylated benzenium species as opposed to the *para*-methylated compound,[35] and therefore the 1,1,2-trimethylnaphthalenium ion is used as a starting point for 2 additional reactions. An exocyclic deprotonation resulting in the formation of a double bond and a final exocyclic (sidechain) methylation are considered (Scheme 3). These reactions form the onset of the sidechain route.

The rate coefficients show that the exocyclic deprotonation is slower than the deprotonation of a ring carbon atom due to a substantially larger energy barrier (Table 1). The final methylation reaction results in the largest compound investigated in
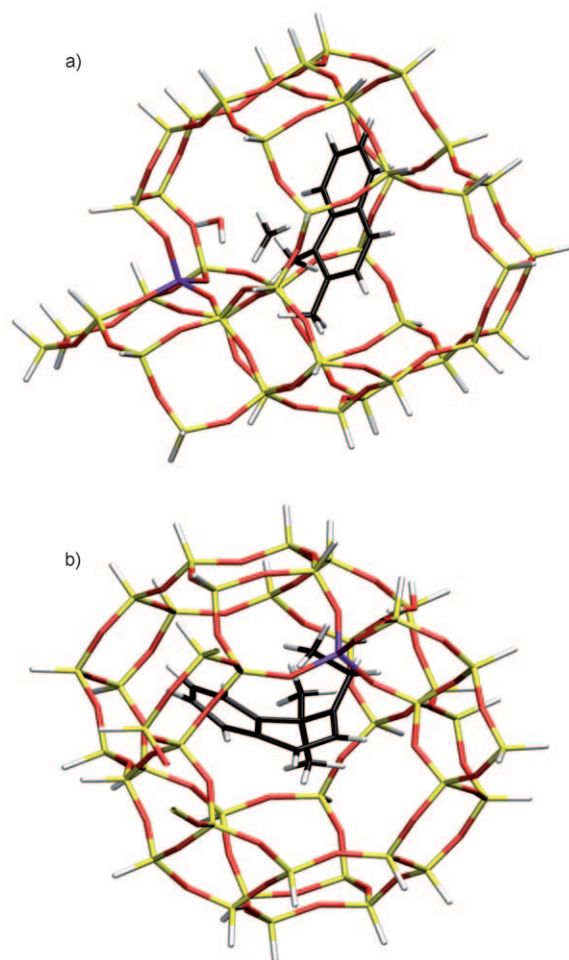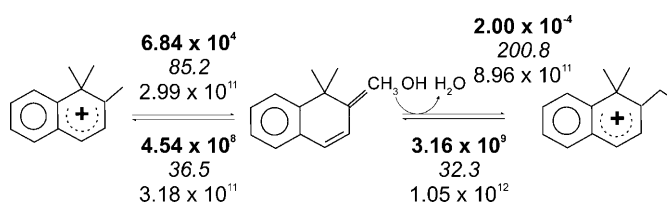

Figure 2. Optimized geometries in the 46T cluster: a) Transition state of the $\alpha'\beta$ *ipso*-methylation; b) product state of the exocyclic methylation.

Scheme 3. Exocyclic deprotonation and methylation of the 1,1,2-trimethylnaphthalenium ion; rate constants k at 670 K (bold) are given in s^{-1}, activation barriers E_a (italics) in kJ mol^{-1}, and pre-exponential factors A in s^{-1}.

this study and clearly challenges the dimensions of the zeolite pore. The calculated barrier and reaction energy are found to be the highest of all reactions investigated in this study. These results suggest that the sidechain path is not an active ethene-producing path for naphthalenic HP species since the CHA cage is found to impose constraints on the transition and product state. The optimized geometry of the latter shows a curled up structure for the bicyclic compound (Figure 2 b). Moreover, we recently came to the same conclusion for benzenic HP species in H-ZSM-5.[35] These results show that even for small- or medium-pore systems, bicyclic compounds should

be regarded as coke precursors rather than active compounds within the sidechain mechanism, as transition and product shape selectivity prohibit the subsequent reactions.

Van der Waals contributions

Since the investigated naphthalenic compounds are bulky organics, van der Waals effects become important. The contributions to the reaction barriers and energies are listed in Table 1. Not surprisingly, the contributions to the energy barriers amount to a decrease of ± 20 kJ mol^{-1} in the case of methyl additions. For deprotonation reactions, the van der Waals corrections on the reaction energies are smaller, and the small positive values result from the more compact product compared to the reactant structure. The large van der Waals correction for the reaction energy, in the case of the methyl addition to the exocyclic double bond, indicates the bulkiness of the product state (Figure 2). Although not negligible, the qualitative picture is not altered by incorporating van der Waals corrections. The influence of the dispersion contributions on the rate coefficients at 670 K is further exemplified (see the Supporting Information, Table S1). The largest effect is found in the case of the $\alpha'\beta$ *ipso*-methylation, for which the rate coefficient of the forward reaction is enlarged by a factor of 226.

Comparison with benzenic HP species

Comparison with the benzenic species (i.e., traditional HP species) is not straightforward as little computational information is available for the CHA topology. We previously calculated the *ipso*-methylation of hexamethylbenzene (HMB),[18] and the reaction barrier and reaction energy for HMB were found to equal 60.8 and -8.4 kJ mol^{-1}. Not surprisingly, these values differ to a large extent from those obtained in this work and point out the differences between the presence of additional methyl groups versus an extra aromatic ring. To allow a more direct comparison, we calculated the *ipso*-methylation of *ortho*-xylene, which can directly be compared with the $\alpha'\beta$ *ipso*-methylation of the bicyclic compound. The reaction barrier at 0 K amounts to 129.3 kJ mol^{-1}, which is indeed smaller than its bicyclic counterpart of 170.2 kJ mol^{-1} (Table 1). The reaction energies are 81.2 and 113.4 kJ mol^{-1} for the benzenic and naphthalenic compound, respectively. The rate coefficients of the forward reactions differ by four orders of magnitude (1.61×10^2 versus 3.77×10^{-2} s^{-1}), whereas the reverse reactions occur at similar rates (3.31×10^7 versus 2.54×10^7 s^{-1}).

Conclusions

We have demonstrated, by means of ab initio computations, that the growth of naphthalenic compounds within a zeolite with chabazite topology is feasible through successive methylation reactions although the rates are smaller compared to benzenic compounds. Our results are in line with earlier experimental observations.

Trimethylated bicyclic molecules should still be considered as active HP intermediates for the MTO process since steric effects between the bulky organic compounds, on one hand, and the zeolite framework on the other hand, do not prohibit the formation of reactive intermediates. This study also indicates that the sidechain mechanism should not be considered as an active ethene-producing cycle for naphthalenic hydrocarbon pool species within the MTO process.

Computational Methods

The investigated zeolite is of the CHA topology and a 46T cluster (with the active site represented by a 8T high level region) was applied. The models were constructed using Zeobuilder.[36] The computations are performed with the Gaussian 03 package[37] using a well-established multilayered method, which combines a ONIOM(b3lyp/dgtzvp:hf/dgtzvp) energy and ONIOM(b3lyp/dgtzvp: MNDO) geometry. Due to the size of our HP species and cluster model, van der Waals contributions were taken into account by using the DFT-D approach as implemented in the Orca software package.[38] Using the optimized ONIOM(b3lyp/dgtzvp:MNDO) geometries, the b3lyp-d method was used to quantify the order of magnitude of the dispersion interactions. In this method, the dispersive energy is described by damped interatomic potentials of the form $C_6 R^{-6}$.[39,40] Rate coefficients and kinetic parameters were computed applying transition state theory as implemented in the TAMkin program, which is a post-processing toolkit for thermochemistry and kinetics analyses.[29–31] For the computation of the kinetic properties, the ONIOM energies (without consideration of the van der Waals corrections) were used. The influence of the dispersion corrections on the rate coefficients can be found in the Supporting Information (Table S1).

[1] M. Stöcker, *Microporous Mesoporous Mater.* **1999**, *29*, 3.
[2] J. F. Haw, W. G. Song, D. M. Marcus, J. B. Nicholas, *Acc. Chem. Res.* **2003**, *36*, 317.
[3] B. Yilmaz, U. Müller, *Top. Catal.* **2009**, *52*, 888.
[4] Z.-M. Cui, Q. Liu, Z. Ma, S.-W. Bian, W.-G. Song, *J. Catal.* **2008**, *258*, 83.
[5] S. Teketel, S. Svelle, K. P. Lillerud, U. Olsbye, *ChemCatChem* **2009**, *1*, 78.
[6] W. G. Song, D. M. Marcus, H. Fu, J. O. Ehresmann, J. F. Haw, *J. Am. Chem. Soc.* **2002**, *124*, 3844.
[7] D. M. Marcus, K. A. McLachlan, M. A. Wildman, J. O. Ehresmann, P. W. Kletnieks, J. F. Haw, *Angew. Chem.* **2006**, *118*, 3205; *Angew. Chem. Int. Ed.* **2006**, *45*, 3133.
[8] D. Lesthaeghe, V. Van Speybroeck, G. B. Marin, M. Waroquier *Angew. Chem.* **2006**, *118*, 1746; *Angew. Chem. Int. Ed.* **2006**, *45*, 1714.
[9] I. M. Dahl, S. Kolboe, *Catal. Lett.* **1993**, *20*, 329.

[10] I. M. Dahl, S. Kolboe, *J. Catal.* **1994**, *149*, 458.

[11] I. M. Dahl, S. Kolboe, *J. Catal.* **1996**, *161*, 304.

[12] R. M. Dessau, *J. Catal.* **1986**, *99*, 111.

[13] S. Svelle, F. Joensen, J. Nerlov, U. Olsbye, K. P. Lillerud, S. Kolboe, M. Bjørgen, *J. Am. Chem. Soc.* **2006**, *128*, 14770.

[14] M. Bjørgen, F. Joensen, K.-P. Lillerud, U. Olsbye, S. Svelle, *Catal. Today* **2009**, *142*, 90.

[15] D. M. McCann, D. Lesthaeghe, P. W. Kletnieks, D. R. Guenther, M. J. Hayman, V. Van Speybroeck, M. Waroquier, J. F. Haw, *Angew. Chem.* **2008**, *120*, 5257; *Angew. Chem. Int. Ed.* **2008**, *47*, 5179.

[16] N. Hazari, J. A. Labinger, V. J. Scott, *J. Catal.* **2009**, *263*, 266.

[17] D. Lesthaeghe, V. Van Speybroeck, M. Waroquier, *Phys. Chem. Chem. Phys.* **2009**, *11*, 5222.

[18] D. Lesthaeghe, B. De Sterck, V. Van Speybroeck, G. B. Marin, M. Waroquier, *Angew. Chem.* **2007**, *119*, 1333; *Angew. Chem. Int. Ed.* **2007**, *46*, 1311.

[19] J. W. Park, G. Seo, *Appl. Catal. A* **2009**, *356*, 180.

[20] J. W. Park, J. Y. Lee, K. S. Kim, S. B. Hong, G. Seo, *Appl. Catal. A* **2008**, *339*, 36.

[21] F. Bleken, M. Bjørgen, L. Palumbo, S. Bordiga, S. Svelle, K.-P. Lillerud, U. Olsbye, *Top. Catal.* **2009**, *52*, 218.

[22] H. Fu, W. Song, J. F. Haw, *Catal. Lett.* **2001**, *76*, 89.

[23] W. Song, H. Fu, J. F. Haw, *J. Phys. Chem. B* **2001**, *105*, 12839.

[24] J. F. Haw, D. M. Marcus, *Top. Catal.* **2005**, *34*, 41.

[25] M. Bjørgen, U. Olsbye, S. Kolboe, *J. Catal.* **2003**, *215*, 30.

[26] L. Palumbo, F. Bonino, P. Beato, M. Bjørgen, A. Zecchina, S. Bordiga, *J. Phys. Chem. C* **2008**, *112*, 9710.

[27] D. Mores, E. Stavitski, M. H. F. Kox, J. Kornatowski, U. Olsbye, B. M. Weckhuysen, *Chem. Eur. J.* **2008**, *14*, 11320.

[28] B. P. C. Hereijgers, F. Bleken, M. H. Nilsen, S. Svelle, K.-P. Lillerud, M. Bjørgen, B. M. Weckhuysen, U. Olsbye, *J. Catal.* **2009**, *264*, 77.

[29] TAMkin is available at http://molmod.ugent.be/code.

[30] A. Ghysels, D. Van Neck, V. Van Speybroeck, T. Verstraelen, M. Waroquier, *J. Chem. Phys.* **2007**, *126*, 224102.

[31] A. Ghysels, V. Van Speybroeck, T. Verstraelen, D. Van Neck, M. Waroquier, *J. Chem. Theory Comput.* **2008**, *4*, 614.

[32] M. Brändle, J. Sauer, *J. Am. Chem. Soc.* **1998**, *120*, 1556.

[33] E. P. Hunter, S. G. Lias, *J. Phys. Chem. Ref. Data* **1998**, *27*, 413.

[34] M. Eckert-Maksić, I. Antol, M. Klessinger, Z. B. Maksić, *J. Phys. Org. Chem.* **1999**, *12*, 597.

[35] D. Lesthaeghe, A. Horré, M. Waroquier, G. B. Marin, V. Van Speybroeck, *Chem. Eur. J.* **2009**, DOI: 10.1002/chem.200901723.

[36] T. Verstraelen, V. Van Speybroeck, M. Waroquier, *J. Chem. Inf. Model.* **2008**, *48*, 1530.

[37] *Gaussian 03*, Revision C.02, M. J. Frisch, G. W. Trucks, H. B. Schlegel, G. E. Scuseria, M. A. Robb, J. R. Cheeseman, J. A. Montgomery, Jr., T. Vreven, K. N. Kudin, J. C. Burant, J. M. Millam, S. S. Iyengar, J. Tomasi, V. Barone, B. Mennucci, M. Cossi, G. Scalmani, N. Rega, G. A. Petersson, H. Nakatsuji, M. Hada, M. Ehara, K. Toyota, R. Fukuda, J. Hasegawa, M. Ishida, T. Nakajima, Y. Honda, O. Kitao, H. Nakai, M. Klene, X. Li, J. E. Knox, H. P. Hratchian, J. B. Cross, V. Bakken, C. Adamo, J. Jaramillo, R. Gomperts, R. E. Stratmann, O. Yazyev, A. J. Austin, R. Cammi, C. Pomelli, J. W. Ochterski, P. Y. Ayala, K. Morokuma, G. A. Voth, P. Salvador, J. J. Dannenberg, V. G. Zakrzewski, S. Dapprich, A. D. Daniels, M. C. Strain, O. Farkas, D. K. Malick, A. D. Rabuck, K. Raghavachari, J. B. Foresman, J. V. Ortiz, Q. Cui, A. G. Baboul, S. Clifford, J. Cioslowski, B. B. Stefanov, G. Liu, A. Liashenko, P. Piskorz, I. Komaromi, R. L. Martin, D. J. Fox, T. Keith, M. A. Al-Laham, C. Y. Peng, A. Nanayakkara, M. Challacombe, P. M. W. Gill, B. Johnson, W. Chen, M. W. Wong, C. Gonzalez, and J. A. Pople, Gaussian, Inc., Wallingford CT, **2004**.

[38] Orca, Version 2.6, An Ab Initio, DFT and Semiempirical Electronic Structure package, F. Neese, University of Bonn, Germany, **2008**.

[39] S. Grimme, *J. Comput. Chem.* **2004**, *25*, 1463.

[40] S. Svelle, C. Tuma, X. Rozanska, T. Kerber, J. Sauer, *J. Am. Chem. Soc.* **2009**, *131*, 816.